Electrochemical properties and electrocatalytic activity of conducting polymer/copper nanoparticles supported on reduced graphene oxide composite

Ali Ehsani [a,*], Babak Jaleh [b], Mahmoud Nasrollahzadeh [a]

[a] Department of Chemistry, Faculty of Science, University of Qom, P.O. Box 37185-359, Qom, Iran
[b] Physics Department, Bu-Ali Sina University, Hamedan 65174, Iran

HIGHLIGHTS

- rGO/CuNPs and polytyramine are prepared by electropolymerization.
- rGO/CuNPs–PT/G shows better capacitance performance.
- rGO/CuNPs–PT/G electrode shows better catalytic performance for methanol oxidation.

ARTICLE INFO

ABSTRACT

Reduced graphene oxide (rGO) was used to support Cu nanoparticles. As electro-active electrodes for supercapacitors composites of reduced graphene oxide/Cu nanoparticles (rGO/CuNPs) and polytyramine (PT) with good uniformity are prepared by electropolymerization. Composite of rGO/CuNPs–PT was synthesized by cyclic voltammetry (CV) methods and electrochemical properties of film were investigated by using electrochemical techniques. The results show that, the rGO/CuNPs–PT/G has better capacitance performance. This is mainly because of the really large surface area and the better electronic and ionic conductivity of rGO/CuNPs–PT/G, which lead to greater double-layer capacitance and faradic pseudo capacitance. Modified graphite electrodes (rGO/CuNPs–PT/G) were examined for their redox process and electrocatalytic activities towards the oxidation of methanol in alkaline solutions. The methods of cyclic voltammetry (CV), chronoamperometry (CA) and electrochemical impedance spectroscopy (EIS) were employed. In comparison with a Cu–PT/G (Graphite), rGO/CuNPs–PT/G modified electrode shows a significantly higher response for methanol oxidation. A mechanism based on the electro-chemical generation of Cu(III) active sites and their subsequent consumptions by methanol have been discussed.

© 2014 Elsevier B.V. All rights reserved.

1. Introduction

Conducting polymers such as polypyrrole, polythiophenes or polyaniline represent a group of conjugated π-electron materials which process a combination of various electrical, optical and other semiconductor properties as an organic semiconductors that with respect to electronic energy levels hardly different from inorganic semiconductors. The electropolymerisation of phenol and phenol derivatives has received considerable attention due to their importance in environmental, industrial electrocatalyst and supercapacitor applications [1–5]. Electrochemistry of the phenol derivatives strongly dependent on the type, position and number of substituents as well as on the chosen experimental conditions. [6,7]. For phenol derivatives with amino groups, the reported voltammetric studies have been interpreted by analogy with the well-established aniline oxidation, i.e. a E(CE)n mechanism; the oxidation of o-aminophenol was described as producing a ladder-structured film and reactive intermediates of 2-amino-phenoxazin-3-1 formation in solution. In the case of tyramine (4-(2-aminoethyl)phenol) (Ty), because the amino function is separated from the phenolic ring by two methylene groups, it is expected that only the phenol moiety is oxidized to perform the polymerization [6,7].

* Corresponding author. Tel.: +98 25 32103038; fax: +98 25 32854973.
E-mail addresses: ehsani46847@yahoo.com, a.ehsani@qom.ac.ir (A. Ehsani).

The optimized molecular structure of polytyramine (heptamer) which obtained from quantum mechanical DFT calculations is presented in Fig. 1.

Graphene nanosheet (GN), which is a monolayer of carbon atoms tightly packed into a honeycomb lattice, has opened a new avenue for utilizing two-dimensional (2D) carbon material as a support because of its high conductivity ($103–104$ S m^{-1}), tremendous surface area (theoretically calculated value, 2630 m^2 g^{-1}), unique graphitized basal plane structure, high thermal and chemical stability, and potential low manufacturing cost [8–10]. These unique structure make graphene a promising additive or supporting component for potential applications in various fields [11–16], such as nanoelectronics [17,18], batteries [19], nanocomposites [20,21], supercapacitors [12], and sensors [22,23] solar cells [24,25] fuel cells [26,27] etc. Especially the metals or metal oxides are distributed onto the surface of graphene or between the graphene layers, as substrates for immobilizing metal or metal oxide catalysts, have been fabricated by restacking graphene sheets in the presence of guest nanoparticles or corresponding precursors. For example, Pt [28], Co$_3$O$_4$ [29] nanoparticles supported by chemically converted graphene were found to be an excellent electrocatalyst for oxygen reduction reaction (ORR). Palladium nanoparticles on graphite oxide and its functionalized graphene derivatives showed high catalytic activities for the Suzuki–Miyaura coupling reaction [11]. TiO$_2$ nanoparticles decorated graphene exhibited high photocatalysis performance [30]. Copper-based and its oxide-based nanomaterials were of great interest for their extensive applications in catalysis, gas sensor, Li ion battery, gas sensor, field-effect transistors and bio-sensors for a long time [31].

Herein, we describe a simple strategy dispersing of rGO/CuNPs within the conducting polymer matrix by in situ electro-polymerization using an ionic surfactant as the supporting electrolyte. The rGO/CuNPs were first dispersed in an aqueous solution containing an ionic surfactant. Then electroactive monomer (Ty) was added into the above mixture and finally electrochemical reaction was preceded at the surface of the graphite electrode. In the present work rGO/CuNPs–PT composite was synthesized by cyclic voltammetry (CV) methods and electrochemical properties of film were investigated by using electrochemical techniques, viz. CV and electrochemical impedance spectroscopy (EIS).

2. Experimental

2.1. Instruments and reagents

All reagents were purchased from the Merck and Aldrich chemical companies and used without further purification. X-ray diffraction measurements were performed with a Philips powder diffractometer type PW 1373 goniometer. It was equipped with a graphite monochromator crystal. Electrochemical studies were carried out in a conventional three electrode cell powered by an electrochemical system comprising of EG&G model 273 potentio-stat/galvanostat and Solartron model 1255 frequency response analyzer. The system is run by a PC through M270 commercial software via a GPIB interface. Saturated Calomel Electrode (SCE), a Pt wire and a graphite (G) electrode (0.22 cm^2) were used as the reference, counter and working electrodes, respectively. The X-ray wavelength was 1.5405 Å and the diffraction patterns were recorded in the 2θ range (10–60) with scanning speed of 2°/min. Morphology and particle dispersion was investigated by scanning electron microscopy (SEM) (Cam scan MV2300). The chemical composition of the prepared nanostructures was measured by EDS performed in SEM. All studies were carried out at 298 ± 2 K.

2.2. Preparation of graphene oxide

Graphene oxide was synthesized from commercial graphite by modified Hummers method [32,33]. The commercial graphite powder (10 g) was put into 230 mL concentrated H$_2$SO$_4$ that had been cooled to bellow of 20 °C with a circulator. 300 g potassium permanganate (KMnO$_4$) was added with stirring, so that the temperature of the mixture was fixed at bellow of 20 °C. Then, the temperature of the reaction was changed and brought to 40 °C and mixture was stirred at 40 °C for 1 h. 500 mL de-ionized water was added to the mixture, causing an increase in temperature to 100 °C. After that, 2.5 mL H$_2$O$_2$ (30 wt. %) was slowly added to the mixture supplementary this solution was diluted by addition lit de-ionized water. For purification, the suspension was washed with 1:10 HCl solution (200 mL) in order to remove metal ions by filter paper and funnel. The suspension was washed with much de-ionized water at several times, until the filtrate became neutral to remove remaining salt impurities. The graphene oxide was characterized by XRD and FT-IR spectroscopy [34].

2.3. Preparation of reduced graphene oxide (rGO)

Chemical reduction of graphene oxide to reduced graphene oxide was done according to a new procedure. Suspension aqueous colloids of GO were prepared from the dried graphene oxide (GO) by mechanical stirring and heat treatment with a circulator. In the experiment, 10 g of graphene oxide was stirred into 1 L of distilled water. This dispersion was stirred using a Fisher mechanical stirring until it became a clear solution with no visible particulate material. After that, the pH of the solution was increased to 10 by adding
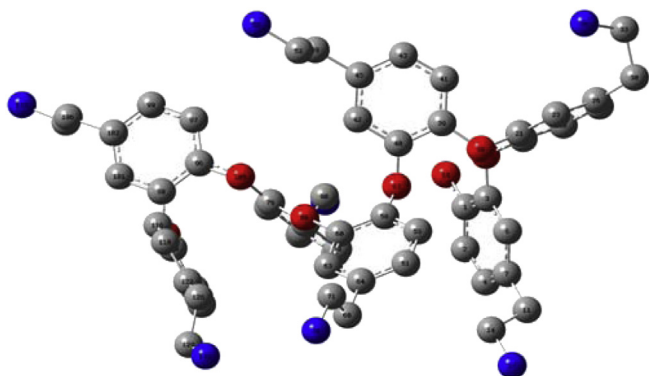

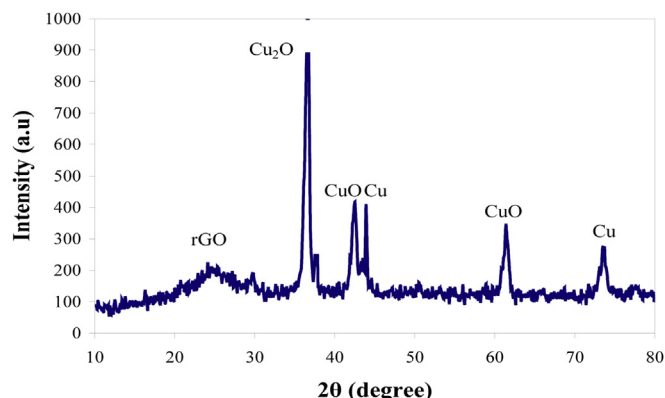**Fig. 1.** Optimized molecular structure of heptamer, H atoms has been omitted for clarity.

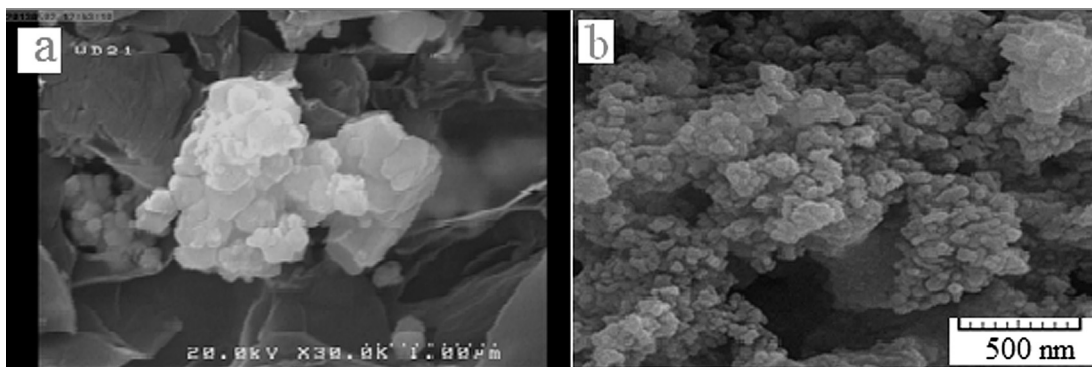**Fig. 2.** XRD pattern of rGO/CuNPs.

Fig. 3. (a) SEM images of rGO/CuNPs and (b) rGO/CuNPs/PT.

NaOH solution and 20 mL of hydrazine monohydrate was added, to the solution at 95 °C and stirred for 4 h, subsequently the reaction was completed, the reduced graphene oxide was collected by filtration as a black powder. The obtained powder was washed with distilled water several times to until the pH is nearly 7 and until to remove the excess hydrazine. The final product was dried in a vacuum oven at 100 °C for 24 h.

2.4. Preparation of CuNPs

200 mL NaOH (2 M) solution was added slowly to the 100 mL $CuSO_4 \cdot 5H_2O$ (2 M) solution and the reaction mixture was heated to 80 °C under constant severe stirring. Copper hydroxide ($Cu(OH)_x$) and copper oxide (CuO_x) was formed and deposited as sediments. Then, the sediments were filtered and recovered. Distilled water and glucose was added to obtained precipitate and agitated until the color of the solution changed into dark red. Glycine (NH_2-CH_2-COOH) was then added to the above solution and the mixture was ultrasonicated for the appropriate time. 100 mL $NaBH_4$ (24 M) solution was then added dropwise to the above solution. After the completion of reaction and allowing the mixture to cool to room temperature, the reaction mixture was filtered, washed with distilled water, after that dried it at 110 °C in a vacuum dryer. The molar ratio of the mixture $Cu^{+2}:NaOH:Glycine:NaBH_4$ are 1:2:1:12 respectively [35–37].

2.5. Preparation of rGO/CuNPs

In a typical procedure, rGO powder and deionized (DI) water were mixed in a 500 mL three-necked flask, and the mixture was ultrasonicated for 45 min at room temperature. Cu nanoparticle was then added slowly to the above mixture solution under continuous stirring at 110 °C for 12 h. Subsequently, the mixture was filtered and washed several times with DI water to remove byproducts. The resulting product dried at 100 °C for 12 h under vacuum to obtain the chemically reduced graphene supported copper nanoparticles (rGO/CuNPs).

2.6. Preparation of rGO/CuNPs/PT

Films of polytyramine were formed on the graphite surface using a tyramine monomer solution (0.01 M tyramine in 0.1 M $LiClO_4$ and 0.1 M $HClO_4$) and (0.01 M tyramine in 0.1 M $LiClO_4$, 0.1 M $HClO_4$, 0.005 M SDS and 1% rGO/CuNPs) under ultrasonic irradiation. The electropolymerization was carried out by potential cycling 40 cycles at a scan rate of 50 mV s^{-1} between −0.2 and 0.9 V versus SCE. In order to incorporate Cu (II) ions into the PT composite, the freshly electropolymerised graphite electrode was placed at open circuit in a well stirred aqueous solution of 0.1 mol L^{-1} Cu (NO$_3$)$_2$.

3. Results and discussion

3.1. Characterization of rGO/CuNPs

The phase and crystallinity of the catalyst were determined by powder X-ray diffraction (XRD). The X-ray diffraction pattern of as synthesized rGO/CuNPs shows the presence of metallic copper and cuprous oxide phases. Fig. 2 shows two broad peaks of 2θ values 43.5° and 50.4° which are assigned to the (111) and (200) indices of face centered cubic (fcc) lattice of metallic Cu. The presence of cuprous oxide could be because of the air oxidation of copper during drying. Peaks at 42.6° and 62.6° could be attributed to cuprous oxide. rGO exhibits a broad peak (002) at about of $2\theta = 25°$ [38]. Moreover, the characteristic peak of GO at 10.7° (001) disappeared in the pattern of the rGO/CuNPs. These results indicated
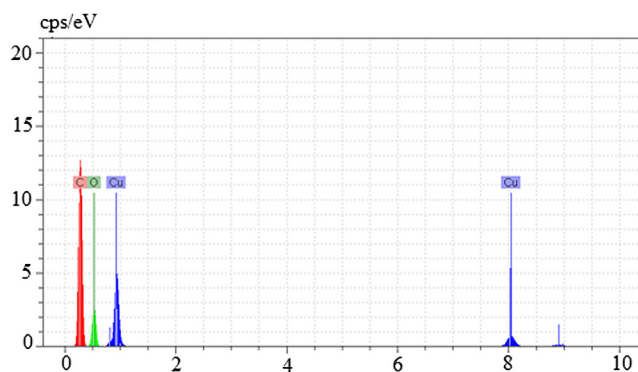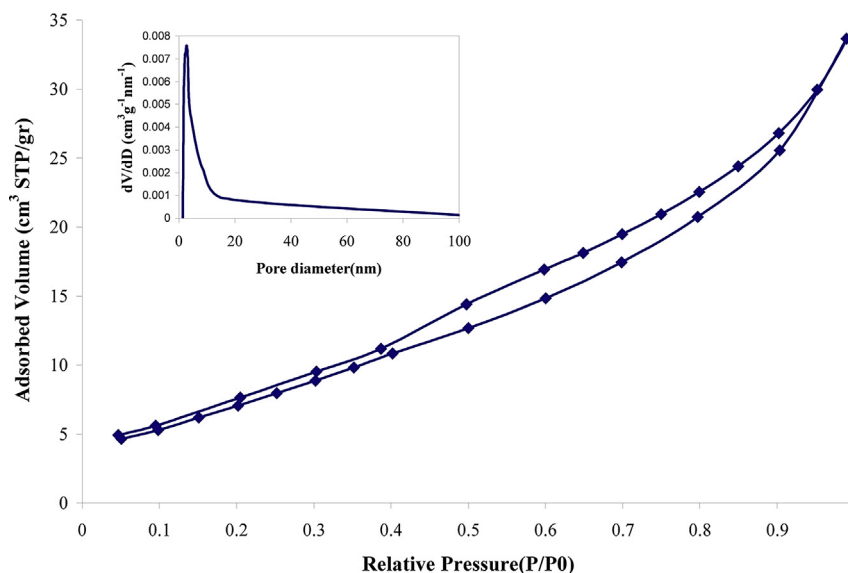

Fig. 4. EDS spectrum of rGO/CuNPs.

Fig. 5. The N$_2$ adsorption–desorption isotherm and Barrett–Joyner–Halenda (BJH) pore size distribution plot of catalyst.

that graphene oxide (GO) was successfully reduced to rGO during the redox reaction.

Fig. 3 shows the Scanning electron microscopic (SEM) images of rGO/CuNPs and rGO/CuNPs/PT. SEM image of rGO/CuNPs (Fig. 3a) showed that uniform 90 nm sized copper nanoparticles were produced. It is clearly observed that the Cu grain pervaded between rGO sheets, which displays a good combination between rGO sheet and CuNPs. SEM image of rGO/CuNPs/PT composite (Fig. 3b) show porous structure with high active surface area. Energy dispersion spectroscopy (EDS) was recorded and shown in Fig. 4. In the EDS spectrum of rGO/CuNPs, peaks related to C, O and Cu were observed.

The surface area of rGO/CuNPs was determined by BET. The N$_2$ adsorption–desorption isotherm and Barrett–Joyner–Halenda (BJH) pore size distribution plot of rGO/CuNPs showed in Fig. 5. The

BET (Brunauer–Emmett–Teller) surface area and single point total pore volume are 29.96 m^2 g^{-1} and 5.2 × 10^{-2} cc g^{-1}, respectively.

3.2. Electrosynthesis of composite film and electrochemical properties

In previous publications [1–5], we described how poly ortho aminophenol films were deposited in situ electropolymerised on the surface of graphite electrode by using of cyclic voltammetry methods. In this study the electropolymerization of Ty was carried out by potential cycling (40 cycles at a scan rate of 50 mV s^{-1}) between −0.2 and 0.9 V versus SCE in the monomer solution containing dispersed rGO/CuNPs. Fig. 6a shows the typical multi-sweep cyclic voltammograms during Ty electro-polymerization in
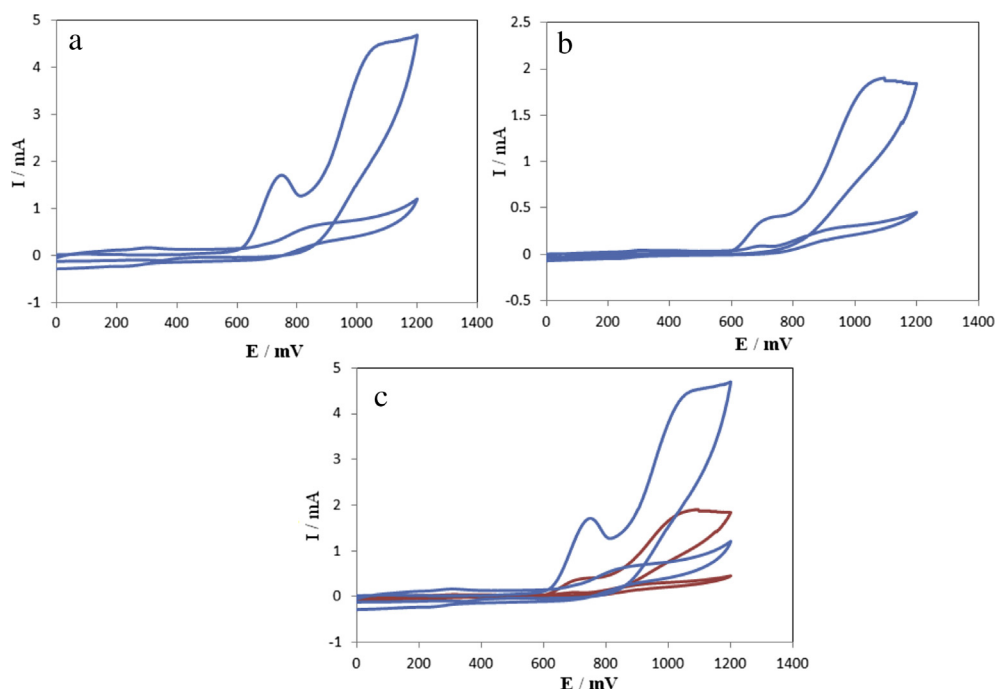

Fig. 6. The typical multi-sweep cyclic voltammograms during electropolymerization of PT in the absence (a) and presence of rGO/CuNPs. (c) Present compared voltammograms of (a) and (b).
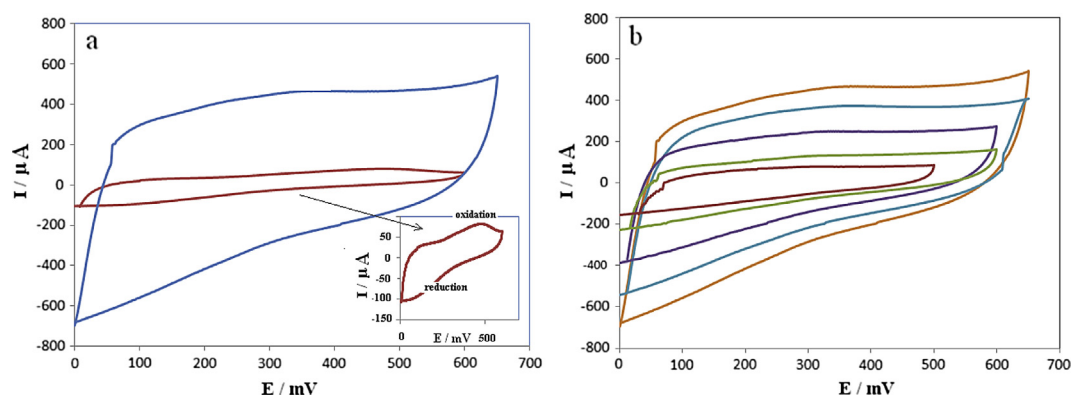
Fig. 7. (a); The cyclic voltammograms of the rGO/CuNPs−PT/G and PT films. (b) The cyclic voltammograms of the rGO/CuNPs−PT/G in different scan rates (25−200 mv s^{-1}). Inset shows different magnification of PT cyclic voltammogram.

the absence of rGO/CuNPs. As shown in Fig. 6a, Tyramine (Ty) is oxidized irreversibly around 900 mV without corresponding cathodic processes in the reverse scan. During the next cycles, a redox peak appeared at lower potential, and its current did not increase considerably with potential cycling. Also, the monomer oxidation potential was shifted and its oxidation current increased (Fig. 6b), while adding rGO/CuNPs to the monomer solution. Under ultrasonic irradiation, the aggregates of rGO/CuNPs were broken down and nanoparticles redispersed in the aqueous solution at nano scale, while at the same time, Ty monomer is polymerized and the synthesized PT absorbed on the surface of nanocrystalline rGO/CuNPs. The surfactant molecules are absorbed on the surface of composite particles and obtained a stabilizing effect.

To elucidate the effect of rGO/CuNPs on the property of PT films, electrochemical performance of composite films was evaluated by carrying out CV measurements in 0.5 M HClO$_4$, as shown in Fig. 7. The cyclic voltammograms of the rGO/CuNPs−PT/G films showed a broad oxidation and reduction waves in positive and negative direction respectively. Their wave currents were stronger than that of pure PT films electrodes. The voltammetric behavior of both films is similar and the CV curves show capacitive-like responses approximately rectangular in shape. The voltammograms reveal the electrodes are stable in HClO$_4$ solution within the sweeping potential range. Close comparisons of CV curves between rGO/CuNPs−PT/G electrode and pure PT/G electrode show that a rGO/CuNPs−PT/G electrode not only displays a higher background current in the potential sweep but also there exist faradic currents, which are believed to arise from the contribution of the loaded rGO/CuNPs. Owing to the higher current in the voltammograms of the rGO/CuNPs−PT/G electrode than a pure PT/G electrode, a larger

capacitance for capacitors equipped with rGO/CuNPs−PT/G electrode can be anticipated. The specific capacitance, SC, can be obtained from the following equation for CV measurements [39−42]:

$$SC = \frac{2i}{sm} \tag{1}$$

where i denotes the average cathodic current, s is the applied potential sweep rate, and m is the mass of each active material on the electrode. Electrode weighting, before and after the deposition process, yields the amount of the active material on the surface of the electrode. It is interesting to see that the supercapacitor made by rGO/CuNPs−PT show a wide open rectangular shaped voltammogram with a charge density of 560 F g^{-1}. Whereas the PT film show nearly rectangular voltammetric shape with maximum specific capacitance of 105 F g^{-1}.

The increase in the current due to increased scan rates show the linear variation in capacitive currents of polymer and composite electrodes as a function of cyclic voltammetric scan rates. Interestingly, the shape of CV curve even at higher scan rate (200 mV s^{-1}) is rectangular and the capacitive current from rGO/CuNPs−PT film is unexpectedly high. The higher slope of the linear trend of CV currents from rGO/CuNPs−PT film is related to formation of hybrid (double layer and pseudo) supercapacitor.

In the case of electrochemical system, EIS can reveal information regarding processes occurring in the polymer matrix when it is doped. This may include kinetic values of the doping process and parameters of the diffusion of ions into the polymers [43−47]. EIS was analyzed for PT films in two different synthesis conditions in acidic solution of HClO$_4$ and LiClO$_4$. Fig. 8 shows the Nyquist
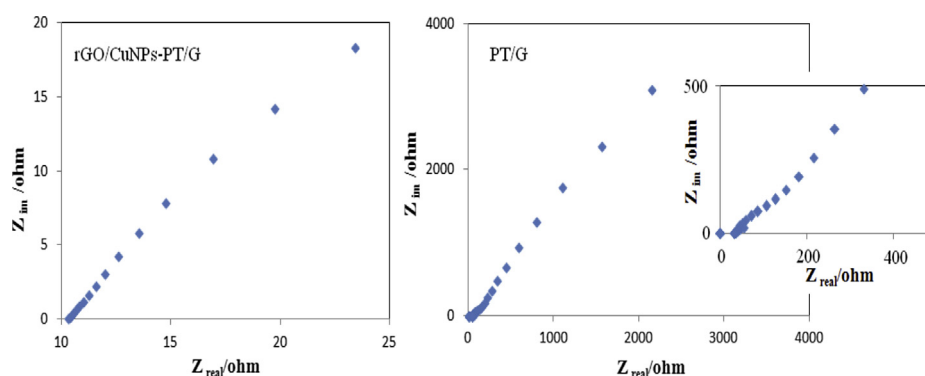

Fig. 8. Nyquist diagrams of rGO/CuNPs−PT/G and PT films in OCP in acidic solution. Inset shows different magnification of Nyquist plot.
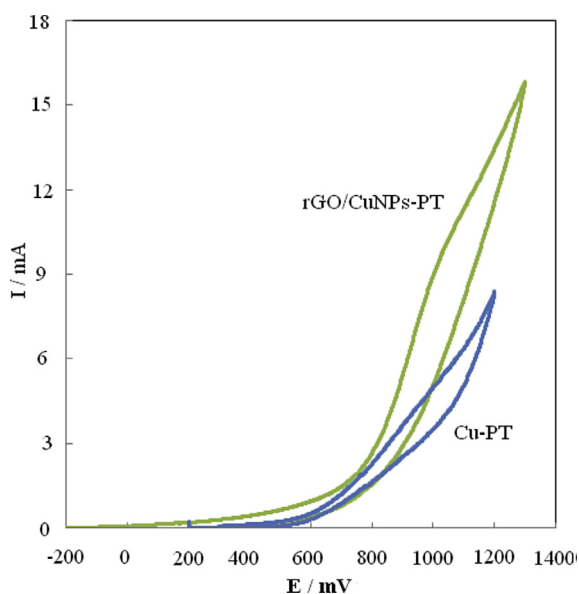
Fig. 9. Cyclic voltammograms of rGO/CuNPs−PT/G and Cu/PT electrode in 0.1 M NaOH solution in the presence of 0.02 M methanol at a potential sweep rate of 10 mV s^{-1}.

improvement effect, which makes the composites have more active sites for faradic reactions and a larger specific capacitance than pure PT. Also, this result in enhanced electric conductivity, lowers the resistance, and facilitates the charge-transfer of the composites.

Composite films were applied to electrooxidation of methanol in alkaline media. Fig. 9a shows cyclic voltammograms of rGO/CuNPs−PT/G electrode in 0.1 M NaOH solution in the presence of 0.02 M methanol at a potential sweep rate of 10 mV s^{-1}. The larger methanol response at the rGO/CuNPs−PT/G respect Cu−PT/G (Fig. 9b) electrode is proposed to be the rGO/CuNPs−PT enhances the catalytic properties of copper oxide through fine dispersion of the catalyst particles into the conductive polymer matrix to results in a drastic increase in surface area.

At rGO/CuNPs−PT/G electrode, oxidation of methanol appeared as a typical electrocatalytic response in alkaline media by Cu(OH)$_2$/CuOOH [48]. The anodic electrochemical reactions can be summarized as follows [48]:

$$Cu^{2+} \rightleftarrows Cu^{3+} + e^- \tag{2}$$

$$Cu^{3+} + CH_3OH_{ads} \rightleftarrows Cu^{2+} + intermediate \tag{3}$$

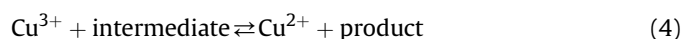$$Cu^{3+} + intermediate \rightleftarrows Cu^{2+} + product \tag{4}$$

Fig. 10a presents the Nyquist diagrams of rGO/CuNPs−PT/G and Cu−PT/G electrodes recorded at 700 mV dc-offset both in the presence of methanol in 0.1 M NaOH solution. Both of the electrode resistance and charge transfer resistance significantly decrease in the presence of rGO/CuNPs in the polymer films. In other words, the bulk-film transport of electrons and the charge transfer resistance (R_{ct}) of rGO/CuNPs−PT composite films are much lower than that of the Cu−PT films in the electrooxidation of the methanol.

Fig. 10b presents the Nyquist diagrams of rGO/CuNPs−PT/G in different concentration of the methanol. In the methanol's concentration range of 0.005−0.02 M a steady decrease of the diameter of the semi-circle is witnessed. Diagrams consist of a small semi-circle terminated to depressed capacitive semicircles at low frequency end of the spectrum. The equivalent circuit compatible with the Nyquist diagram recorded in the presence of methanol was depicted in Fig. 10b. To obtain a satisfactory impedance simulation of ethanol electro-oxidation, it is necessary to replace the capacitor C with a constant phase element (CPE) in the equivalent circuit. The most widely accepted explanation for the presence of CPE behavior and depressed semicircles on solid electrodes is microscopic
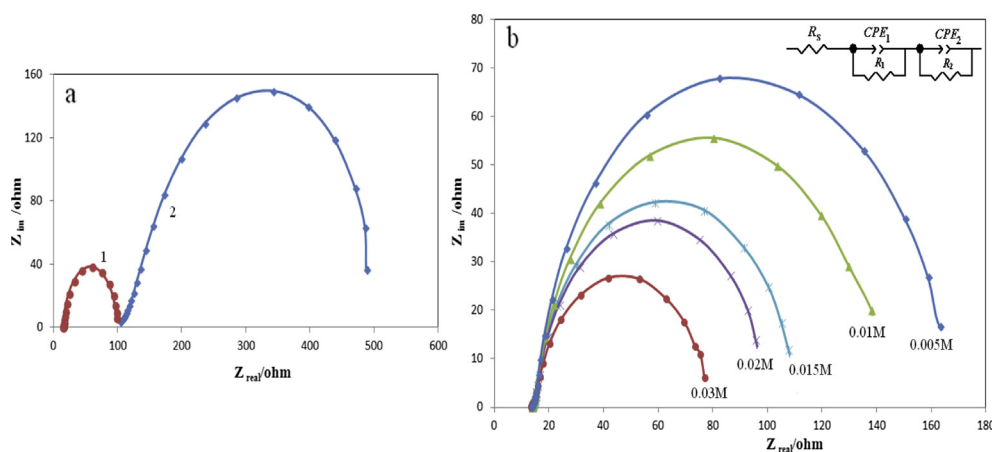
diagrams of electrodes in open circuit potential (OCP). The plot in Fig. 8 depicts a single semi-circle in the high frequency region and a straight line in the low-frequency region for all spectra. The high-frequency arc is the overall contact impedance generated from the electrical connection between rGO/CuNPs−PT/G composites and the backing plate as well as the charge transfer at the contact interface between the electrode and the electrolyte solution. In spite of the similar shape of the impedance spectra, there is an obvious difference between the diameters of the semi-circles. That is, the diameters of the semicircles decline greatly in the presence of rGO/CuNPs in the PT. In other words, the bulk-film transport of electrons and the charge transfer resistance (R_{ct}) of rGO/CuNPs−PT composite films are much lower than that of the pure PT films. This means that the rGO/CuNPs inside the PT matrix may lead to a faster electron transport in the bulk-film and charge transfer in the parallel PT film/solution interface and rGO/CuNPs/solution interface, compared to that in the originally single PT film/solution interface. This fact may suggest that the rGO/CuNPs has an obvious

Fig. 10. (a)Nyquist diagrams of rGO/CuNPs−PT and Cu−PT/G electrodes recorded at 700 mV dc-offset both in the presence of methanol in 0.1 M NaOH solution. (b) Nyquist diagrams of rGO/CuNPs−PT in different concentration of the methanol.
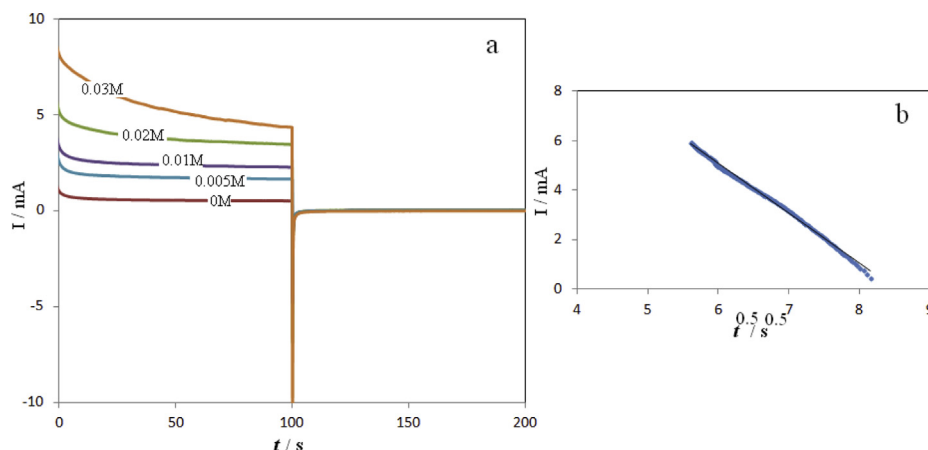
Fig. 11. (a) Double steps chronoamperogram of rGO/CuNPs–PT electrode in 0.1 M NaOH solution with different concentrations of methanol. (b) Dependency of transient current on $t^{1/2}$ for 0.02 M methanol in the surface of rGO/CuNPs–PT electrode.

roughness, causing an inhomogeneous distribution in the solution resistance as well as in the double-layer capacitance. The parallel combination of charge transfer resistance R_1 and constant phase element CPE_1 accounts for the injection of electrons from the conductive polymer to the back metallic contact. R_2 and CPE_2 represent the methanol oxidation. As increasing methanol concentrations decrease the diameters of semicircle, and charge transfer for methanol electrooxidation on the surface of rGO/CuNPs–PT/G is lower than Cu–PT. In other words, introduction of rGO/CuNPs into the polymer matrix decrease the charge transfer resistance in Nyquist plots.

Chronoamperograms were recorded by setting the working electrode potentials to the desired values and measuring the catalytic rate constant on the rGO/CuNPs–PT/G electrode surface. Fig. 11a shows chronoamperograms for the rGO/CuNPs–PT/G electrode in the absence and presence of methanol over the concentration range 0.005–0.02 M. Plotting the net currents versus the square roots of time results in linear dependencies (Fig. 11b). Therefore, a diffusion-controlled process is dominant for electrooxidation of methanol. By using the slopes of these lines, we can obtain the diffusion coefficients of the methanol according to the Cottrell equation [49]:

$$I = nFAD^{1/2}C^*\pi^{-1/2}t^{-1/2} \qquad (5)$$

where D is the diffusion coefficient, and C^* is the bulk concentration. The mean values of the diffusion coefficients for methanol were 8.52×10^{-6} cm^2 s^{-1} on the rGO/CuNPs–PT surface. Chronoamperometry can also be used to evaluate the catalytic rate constant according to [49]:

$$\frac{I_{cat}}{I_L} = \gamma^{1/2}\left[\pi^{1/2}\mathrm{erf}\left(\gamma^{1/2}\right) + \exp(-\gamma)/\gamma^{1/2}\right] \qquad (6)$$

where I_{cat} and I_L are the currents in the presence and absence of the methanol, respectively, and $\gamma = k_0 C t$ is the argument of the error function. k_0 is the catalytic rate constant, and t is elapsed time. In cases where $\gamma > 1.5$, $\mathrm{erf}(\gamma^{1/2})$ is almost equal to unity, and Eq. (6) can be reduced to

$$\frac{I_{cat}}{I_L} = \gamma^{1/2}\pi^{1/2} = \pi^{1/2}(kC_M t)^{1/2} \qquad (7)$$

From the slopes of the I_{cat}/I_L versus $t^{1/2}$ plots, the mean values of k_0 obtained for methanol was 7.39×10^3 cm^3 mol^{-1} s^{-1}.

4. Conclusions

We have demonstrated a simple and general strategy, namely in situ electropolymerization by using the ionic surfactant as electrolyte, for dispersing rGO/CuNPs within conducting films. In comparison with a polymer the rGO/CuNPs–PT/G electrode shows a better catalytic performance for the electrocatalytic oxidation of methanol. The results show that, the rGO/CuNPs–PT/G has better capacitance performance. This is mainly because of the really large surface area, and the better electronic and ionic conductivity of rGO/CuNPs–PT/G, which lead to greater double-layer capacitance and faradic pseudo capacitance.

Acknowledgment

References

[1] M.G. Mahjani, A. Ehsani, M. Jafarian, Synth. Met. 160 (2010) 1252.
[2] A. Ehsani, M.G. Mahjani, M. Jafarian, A. Naeemy, Prog. Org. Coat. 69 (2010) 510.
[3] A. Ehsani, M.G. Mahjani, M. Jafarian, Synth. Met. 161 (2011) 1760.
[4] A. Ehsani, M.G. Mahjani, M. Jafarian, Synth. Met. 162 (2012) 199.
[5] A. Ehsani, M.G. Mahjani, M. Bordbar, R. Moshrefi, Synth. Met. 165 (2013) 51.
[6] D. Gonçalves, R.C. Faria, M. Yonashiro, L.O.S. Bulhões, J. Electroanal. Chem. 487 (2000) 90.
[7] A.M. Tenreiro, C. Nabais, J.P. Correia, F.M.S.S. Fernandes, J.R. Romero, L.M. Abrantes, J. Solid State Electrochem. 11 (2007) 1059.
[8] A.K. Geim, K.S. Novoselov, Nat. Mater. 6 (2007) 183.
[9] J.S. Bunch, A.M. Van Der Zande, S.S. Verbridge, I.W. Frank, D.M. Tanenbaum, J.M. Parpia, H.G. Craighead, P.L. McEuen, Science 315 (2007) 490.
[10] S. Park, R.S. Ruoff, Nat. Nanotechnol. 4 (2009) 217.
[11] G.M. Scheuermann, L. Rumi, P. Steurer, W. Bannwarth, R. Mulhaupt, J. Am. Chem. Soc. 131 (2009) 8262.
[12] M.D. Stoller, S.J. Park, Y.W. Zhu, J.H. An, R.S. Ruoff, Nano Lett. 8 (2008) 3498.
[13] Y.X. Xu, L. Zhao, H. Bai, W.J. Hong, C. Li, G.Q. Shi, J. Am. Chem. Soc. 131 (2009) 13490.
[14] X. Wang, L.J. Zhi, K. Mullen, Nano Lett. 8 (2008) 323.
[15] D. Li, M.B. Muller, S. Gilje, R.B. Kaner, G.G. Wallace, Nat. Nanotechnol. 3 (2008) 101.
[16] P.K. Ang, W. Chen, A.T.S. Wee, K.P. Loh, J. Am. Chem. Soc. 130 (2008) 14392.
[17] P. Avouris, Z. Chen, V. Perebeinos, Nat. Nanotechnol. 2 (2007) 605.
[18] Y.W. Son, M.L. Cohen, S.G. Louie, Nature 444 (2006) 347.
[19] P. Guo, H.H. Song, X.H. Chen, Electrochem. Commun. 11 (2009) 1320.
[20] S. Stankovich, D.A. Dikin, G.H.B. Dommett, K.M. Kohlhaas, E.J. Zimney, E.A. Stach, R.D. Pinen, S.T. Nguyen, R.S. Ruoff, Nature 442 (2006) 282.
[21] S. Guo, S. Dong, E. Wang, ACS Nano 4 (2009) 547.
[22] C.S. Shan, H.F. Yang, J.F. Song, D.X. Han, A. Ivaska, L. Niu, Anal. Chem. 81 (2009) 2378.
[23] Y. Wang, Y. Li, L. Tang, J. Lu, J. Li, Electrochem. Commun. 11 (2009) 889.

[24] X. Wang, L.J. Zhi, N. Tsao, Z. Tomovic, J.L. Li, K. Mullen, Angew. Chem. Int. Ed. 47 (2008) 2990.
[25] J.B. Wu, H.A. Becerril, Z.N. Bao, Z.F. Liu, Y.S. Chen, P. Peumans, Appl. Phys. Lett. 92 (2008) 263302.
[26] E. Yoo, T. Okata, T. Akita, M. Kohyama, J. Nakamura, I. Honma, Nano Lett. 9 (2009) 2255.
[27] Y.C. Si, E.T. Samulski, Chem. Mater. 20 (2008) 6792.
[28] A.C. Chen, P. Holt-Hindle, Chem. Rev. 110 (2010) 3767.
[29] S.B. Yang, X.L. Feng, S. Ivanovici, K. Mllen, Angew. Chem. Int. Ed. 49 (2010) 8408.
[30] D.H. Wang, D.W. Choi, J. Li, Z.G. Yang, Z.M. Nie, R. Kou, D.H. Hu, C.M. Wang, L.V. Saraf, J.G. Zhang, I.A. Aksay, J. Liu, ACS Nano 3 (2009) 907.
[31] Y. Qian, F. Ye, J. Xu, Z.-G. Le, Int. J. Electrochem. Sci. 7 (2012) 10063.
[32] W.S. Hummers, R.E. Offeman, J. Am. Chem. Soc. 80 (1958) 1339.
[33] N.I. Kovtyukhova, P.J. Ollivier, B.R. Martin, T.E. Mallouk, S.A. Chizhik, E.V. Buzaneva, A.D. Gorchinskiy, Chem. Mater. 11 (1999) 771.
[34] Y. Zhao, X. Song, Q. Song, Z. Yin, CrystEngComm 14 (2012) 6710.
[35] I.B. Jeong, Y.S. Kim, B.Y. Lee, Y.H. Kim, B.S. Jeong, M.S. Lee, Patent Application Publication Pub. No.: US 2004/0221685A1, 2004.
[36] G. Zhao, M.P. Pompeo, Patent Application Publication Pub. No.: US 7517382B2, 2009.
[37] M. Nasrollahzadeh, A. Ehsani, A. Rostami-Vartouni, Ultrason. Sonochem. 21 (2014) 275–282.
[38] Z. Xiong, L.L. Zhang, J. Ma, X.S. Zhao, Chem. Commun. 46 (2010) 6099.
[39] A.L.M. Reddy, S. Ramaprabhu, J. Phys. Chem. C. 111 (2007) 7727.
[40] K. Prasad, N. Miura, J. Power Sources 135 (2004) 354.
[41] W.C. Chen, T.C. Wen, J. Power Sources 117 (2003) 273.
[42] C. Arbizzani, M. Mastragostino, F. Soavi, J. Power Sources 100 (2001) 164.
[43] A. Ehsani, M.G. Mahjani, M. Jafarian, A. Naeemy, Electrochim. Acta 71 (2012) 128.
[44] A. Ehsani, M.G. Mahjani, M. Jafarian, Turk. J. Chem. 35 (2011) 1.
[45] A. Ehsani, M.G. Mahjani, M. Bordbar, S. Adeli, J. Electroanal. Chem. 710 (2013) 29.
[46] A. Ehsani, F. Babaei, M. Nasrollahzadeh, Appl. Surf. Sci. 283 (2013) 1060.
[47] A. Ehsani, S. Adeli, F. Babaei, H. Mostaanzadeh, M. Nasrollahzadeh, J. Electroanal. Chem. 713 (2014) 91.
[48] H. Heli, M. Jafarian, M.G. Mahjani, F. Gobal, Electrochim. Acta 49 (2004) 4999.
[49] A.J. Bard, L.R. Faulkner, Electrochemical Methods, Wiley, New York, 2001.